JCSE The Journal of Corrosion Science and Engineering
ISSN 1466-8858
Volume 5 Preprint 4

Electrochemical behaviour of Fe-36Ni alloy under thin electrolyte layer

A. KADRI[1], C. FIAUD[2], M. OULLADJ[1], L. HAMADOU[1], N. BENBRAHIM[1]

[1] Laboratoire de Matériaux Electrochimie & Corrosion, Faculté des Sciences, Université Mouloud MAMMERI B.P. 17 Tizi-Ouzou 15000 Algeria.
[2]Laboratoire d'Etudes de la Corrosion, ENSCP, 11 rue P. & M. Curie 75231 Paris cedex 05 France.

Abstract

We present in this paper the results of an investigation on the corrosion kinetic of Fe-36Ni alloy in contact with a thin film of solution. We are interested in the potential distribution and the variation of the electrochemical impedance as a function of the electrolyte film thickness. The results obtained show clearly three essential domains with the existence of one zone of characteristic thickness which is near 100 µm

I. Introduction

Many corrosion processes such as pitting, crevice and atmospheric corrosion, take place in restricted volumes of electrolyte. For instance, a thin electrolyte film in contact with a metallic surface could generate a modification in the potential distribution, mass transport, production of metallic cations and hydrolysis reactions. Some effects of specific galvanic couplings (pairings) and local pH variation could result from this particular geometry [1- 4].

The study of electrochemical processes occurring in definite systems could be carried out in simulation cells where the electrolyte layer thickness ε is maintained to a very small value (≥ 20 µm). The potential and the concentration are therefore time and space distributed. The position

of the different electrodes plays therefore a determining role in on the electrochemical features obtained at a steady and non-steady state techniques. Recently, an ac impedance study on corrosion of Al-Zn alloy-coated steel in contact with a thin layer of electrolyte is reported [5]. The authors found that the corrosion current density estimated from the polarisation resistance significantly decreases as the thickness of electrolyte layer increases between 15 and 100 μm and is almost independent of the thickness up to 888 μm.

Several mechanisms and models describing crevice corrosion are reported in previous works [6,7,]. So, Watson and al [8] describe a new mathematical model of the incubation period of crevice corrosion of stainless steels and nickel alloys in chloride solutions. They suggest an other transport process treatment which includes both ionic migration and diffusion. Betts [9] proposes to restate understanding on mechanisms of the crevice corrosion in which the influence of some parameters such as O_2, Cl^-, H^+, inclusions, is to be studied more fittingly. More recently, a novel approach to characterising corrosion within a crevice has been reported by Klassen and al [10]. According to Klassen and al, the presence of a crevice produced a positive shift in the specimen potential that is consistent with an increase in the potential of the controlling anodic reaction due to higher concentrations of dissolution products at the metal surface.

This paper presents the results of an investigation on the corrosion kinetics on Fe-36Ni alloy covered with a thin film of solution consisting of (Na_2SO_4 0.05 M + H_2SO_4 0.05 M). The aim of this study is to determine the potential distribution and the variation of the electrochemical impedance as a function of the electrolyte film thickness.

II. Experimental

A series of experiments has been carried out to characterise the effect of the electrolyte film thickness. For this purpose, the used thin layer cell is represented and described in figure 1.

The working electrode is a cross section rod of 5 mm diameter made of an Fe-36Ni alloy. The electrode is covered with a thermosetting epoxy resin prior to its embedding in an insulating Teflon material so as to avoid any infiltration. The working electrode prepared in this way is located in the cell containing 250 ml of (Na_2SO_4 0.05 M + H_2SO_4 0.05 M) aqueous solution at a pH value of 2.9. The solution is de-aerated by argon bubbling. After one hour, the insulating upper part facing opposite to downwards is moved vertically to obtain the desired thickness of electrolyte layer. During these operations, an argon atmosphere is maintained above the solution.

The apparatus used for electrochemical impedance measurements was a frequency response analyser Solartron 1250 coupled with the electrochemical interface Solartron 1186 allowing a frequency range from 10 kHz to 10 mHz. The working electrode was polarised galvanostatically in order to allow it to raise its corrosion potential. A small amplitude ac current was superimposed in order to measure the complex impedance $Z = \Delta E / \Delta I$ where ΔE is the potential difference between the working electrode and the reference electrode.

III. Results and discussions

III.1. Anodic current-potential curves

The electrochemical behaviour of the Fe-36Ni alloy in the bulk solution has been previously studied [11]. So, The influence of some parameters such as H^+, O_2 and Cl^- was revealed. In order to understand the electrochemical behaviour of the alloy in **c**ircumstances of atmospheric corrosion, it was interesting to observe the evolution of the main electrochemical parameters in accordance with the film thickness in contact with the working electrode.

A series of tests has been carried out to illustrate the effect of the electrolyte film thickness. For this purpose, the thin layer cell used has been described in figure 1. The working

electrode is a 5 mm diameter cross section rod made of Fe-36Ni alloy. The electrode is covered with a thermosetting epoxy resin before its embedding with an insulating Teflon made material in such a way as to avoid any infiltration. The working electrode prepared in this way is located in the cell containing 250 ml of an aqueous solution (Na_2SO_4 0.05 M + H_2SO_4 0.05 M) at a pH value of 2.9. The solution is de-aerated by argon bubbling. After one hour, the insulating upper part facing is moved vertically in order to obtain the required thickness of electrolyte layer. While the atmosphere of argon is being maintained above the solution, the anodic polarisation curve is plotted after ten minutes. The results obtained for different values of electrolyte thickness are summarised in Table 1 and the related curves are shown on Figure 2.

So, it has been noticed a general tendency to the diminution of the current density of the activation peak (Im) and a displacement of the corresponding potential of this peak (Ep) (passivation potential) towards more positive values when the thickness of the electrolyte layer is smaller. These observations could be explained by the two following phenomena:

- the potential drop generated by the equivalent resistance of the electrolyte, which will be described subsequently.

- the accumulation of corrosion products within the isolated electrolyte layer. If this second phenomenon for instance had to be considered, the proportions of iron and nickel in the alloy (64% Fe; 36% Ni, the standard potentials of Fe/ Fe^{2+} and Ni^{2+}/ Ni would be - 0.44 V/ ENH and - 0.23 V/ ENH), respectively ; the anodic polarisation of the working electrode is therefore expressed effectively by the dissolution of iron in solution according to the following global reaction:

$$Fe \rightarrow Fe^{2+} + 2\,e^{-} \quad (1)$$

Indeed, The metallic cations are solvated by the solvent molecules present within the thin layer of solution. In order to characterise the evolution of the concentration corrosion products within the

thin electrolyte layer as the thickness decreases, one can calculate the quantity of iron dissolved in the thin electrolyte layer according to the reaction 1 above.

Thus, bearing in mind, the flux ϕ_R of the electrolysis reaction products on one hand and, the diffusion flux ϕ_D of the corrosion products towards the outside of the thin layer, on the other hand, the integration of the current-potential curves (electrolysis duration: t_0 = 200 seconds) gives thereafter the equivalent quantity of electricity. The number of coulombs per second is then given by the following relation:

$$Q\ (\text{coulombs} / \text{sec}) = \frac{\int_0^{t_0} i\, dt}{t_0} \qquad (2)$$

and the flux of the reaction 1 is given by:

$$\phi_R\ (\text{mole} / \text{sec}) = \frac{Q}{2\,F} \qquad (3)$$

When the thickness ε of the film decreases, a diffusion of the corrosion products towards the bulk solution occurs across a volume which decreases in the same proportions. It is therefore necessary to take into account the diffusion flux in order to display quantitatively the concentration of iron in the thin electrolyte layer. The following relation scheme (4) establishes the proportionality between the diffusion flux ϕ_D and the thickness ε:

$$\phi_D = C(t).\ k.\ \varepsilon \qquad (4)$$

That is:

$$\phi_D = C(t)\,\frac{S.D}{\delta} \qquad (5)$$

with:

$$S = \Pi .d .\varepsilon \qquad (6)$$

The parameters under consideration are:

C (t): concentration of the reaction products

D: diffusion coefficient of Fe^{2+}

S: lateral surface

δ : distance between the edge of the thin layer and the metal surface

d: diameter of the thin layer

K: constant of proportionality.

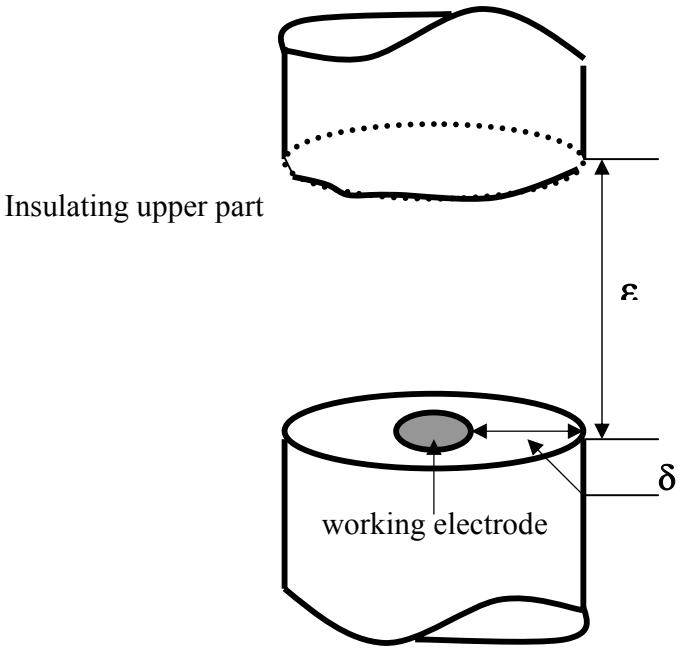

The thin layer cell configuration

The concentration limit of dissolved iron in the thin layer is attained when the rate (ϕ_R) of the reaction (1) becomes equal to the diffusion flux (ϕ_D) of the produced species:

$$\phi_R = \phi_D$$

The calculations have been made with the following equations:

$$C\ (mole.\ cm^{-3}) = \frac{\phi_R}{S\ \frac{D}{\delta}} \qquad [7]$$

$$C\ (mole/l) = \frac{\phi_R\ .\ \delta.\ 10^3}{S.\ D} \qquad [8]$$

The parameters used were:

$D = 10^{-5}\ cm^2.sec^{-1}$

$\delta = 1$ cm

$d = 2$ cm

$t_0 = 200$ sec.

And the results reported in Table 2. They indicate that the concentration increases 20 times when ε changes from 500 to 100 μm and reaches some values of several moles per litre. The molecules of solvent are therefore progressively consumed to hydrate the metallic cations produced at the interface.

The solubility of $FeSO_4$ in H_2SO_4 given in the literature is 1.4 M [12]. After a qualitative measurement, the saturated solution obtained had a concentration of 1.3 M in $FeSO_4$. In order to determine the thickness ε corresponding to the saturation of the solution in the thin layer, an

average concentration of 1.35 M had been considered**,** according to the previous converse calculation, corresponding to an electrolyte thickness of 150 μm.

The accumulation of the corrosion products in the thin layer will hinder the passivation process which could then become more and more difficult. This hypothesis can explain the results obtained for ε < 300 μm (Table 1), for which the activation peak is observed for some important over potential.

When ε < 100 μm, the activation peak on the anodic polarisation curve is not observed. Thus, the alloy remains active in a potential region corresponding to its normally passive state. As the diffusion of the species towards and originating from the outside of the thin layer becomes negligible for these thickness values, the confinement of the corrosion products can accelerate the metal dissolution process according to the following mechanism:

$$Fe \rightarrow Fe^{2+}, n\,H_2O + 2\,e^-$$
$$Fe + m\,H_2O \leftrightarrow \text{Oxide (passive film)}$$

The later states the well-known role of water in the reaction. In other words, if the thin layer becomes poor in water molecules, therefore the equilibrium of the second reaction is shifted to the left and, consequently, the passive film dissolves. In order to better characterise the influence of the thin layer thickness ε on the passivation process of Fe-36Ni alloy, the electrochemical response of this interface by measuring the variation of its complex impedance as a function of frequency has been studied.

2. Electrochemical impedance in a thin electrolyte layer

The working electrode was polarised galvanostatically in order to allow it to adopt its corrosion potential. A small amplitude ac current was superimposed in order to measure the

complex impedance $Z = \Delta E / \Delta I$ where ΔE is the potential difference between the working electrode and the reference electrode.

The impedance diagrams obtained are reported on figure 3. This result illustrates the influence of the layer thickness ε on the electrode impedance. In order to delineate the various frequency domains and the related experimental parameters, a single diagram corresponding to ε = 20 μm has been represented (Figure 4). As shown by the results, in the low frequency domain, the impedance is close to a capacitive arc corresponding to a parallel RC circuit. The extrapolation down to zero frequency gives the charge transfer resistance R_t defined by the arc diameter. The influence of ε on R_t will be discussed subsequently.

As ε is decreased, it can be noted range that a typical feature appears in the high frequency, namely a straight line of slope unity (45°). Therefore if R_D is defined as the contribution of this region to the real part of the impedance, the polarisation resistance will be given by the summation $(R_e + R_D + R_t)$ where R_e is the high frequency limit of the impedance.

The thin layer cell configuration used here gives no ambiguity in ascribing R_e to the resistance of the ring shape electrolyte path outside the working electrode zone and R_D to the ohmic term of the impedance distributed in the electrolyte layer confined between the working electrode and the insulating upper part of the cell .

Figure 5 shows the plot of the reciprocal of the electrolyte resistance R_e as a function of ε; it can be seen that the experimental points fall on a straight line through the origin. This behaviour strongly supports the foregoing interpretation proposed for R_e. It is necessary as well to note that R_D varies in the same sense than R_e. The dependence of R_D upon the layer thickness is in agreement with a radial distribution of current and potential from the periphery to the center of the circular active surface. A similar situation has been thoroughly probed, at least

theoretically, in the studies of porous electrode polarisation [13-17]. It has been shown how a tubular pore could serve for modelling the thin layer configuration cell used [18].

2.1 Influence of the thickness ε on Re

Figure 6 shows the magnification of the high frequency domain of the impedance diagrams previously reported on the figure 3. For $\varepsilon < 200$ µm, the high value of R_e suggests an important ohmic drop which masks the electrochemical reactions to the interface, particularly when the passivation process is imposed to the working electrode. In order to illustrate this phenomenon, the anodic polarisation curves have been recorded in the $20\ \mu m < \varepsilon < 200\ \mu m$ thickness range, by measuring R_e at 10 kHz prior to plotting of each curve. The figure 7 shows that the current-potential curves obtained are linear, thus confirming a strong contribution of a purely ohmic drop. It is necessary to notice the displacement of the corrosion potential (cf. table 3) towards more electronegative values while ε decreases. This behaviour could not exemplify another occurrence than an electrochemical phenomenon. For instance, this tendency presumably expresses a displacement of the anodic elementary curve term towards more important over potentials by favouring the dissolution of the alloy.

The calculated slopes of the recorded polarisation curves yield $P = R_e + R_D$ (table 3). The reciprocal of P has been plotted as a function of ε. The obtained points fall on a straight line through the origin (Figure 8). However, it can be seen from table 3 that P is smaller than the ($R_e + R_D$) value deduced from the impedance diagram.

The R_D effect on the current-potential curves is less evident with regard to the potential and current distribution between the edge and the centre of the thin layer. The precision of the set thickness could be limited by some irregularities of surfaces and/ or by a lack of parallelism

between the two plans delimiting the thin layer. This could explain the gap observed for $\varepsilon < 100$ μm.

In conclusion, it is evident that the strong contribution of the ohmic drop is expressed in a coherent way by the ac impedance measurements as well as by the current-potential curves. On the other hand, the behaviour of the interface has been more clearly identified by the ac impedance measurements in the high frequency domain.

2.2 Influence of the thickness on R_t

The impedance diagrams reported on figure 3 show a high sensitivity of the interface behaviour with the electrolyte layer thickness decreasing. On one hand, the shift of the impedance diagrams to the right is explained in part by the increasing of R_e and, on the other hand, by a distortion of the capacitives arcs resulting from the potential distribution of the interface. Furthermore, the diameter of the capacitive arcs increases. This characterises an increase of R_t (real part limit of the impedance when the frequency tends towards zero).

For $\varepsilon < 100$ μm, an effect converse to the previous one is observed: the diameter of the arc decreases, and this could indicate a diminution of the R_t value (table 4). This is in agreement with an increase of the corrosion rate ($1 / R_t = k. I_{corr}$) [19].

Thereafter, the concentration of the corrosion products in the thin electrolyte layer has been computed as a function of the thickness according to the same principle than the previously stated for the current-potential curves.

The procedure has been started from the transfer resistance R_t by taking the product $R_t . I_{corr} = 30$ mV (working at the corrosion potential).

The results are shown in table 5. It has been noticed that the concentration in Fe^{2+} ions increases ten fold when ε decreases from 500 to 40 μm. This agrees with the results observed under the anodic polarisation.

However the concentration deduced from the measurement at the corrosion potential, is lower than that corresponding to the precipitation of $FeSO_4,7H_2O$. In this case, a precipitation phenomenon of salts at the surface could be invoked in order to explain the influence of the thin layer thickness on the variation of R_t presumed that there is a location of the corrosion phenomenon on this surface starting from a certain electrolyte film thickness.

The local strong current density can cause the formation of satisfactory amount of corrosion product so that precipitation occurs when the electrolyte layer thickness is sufficiently small. Such a hypothesis should be verified at least qualitatively in a first time.

The variation of R_t as a function of ε shown in figure 9 exhibits three domains, namely $\varepsilon > 250$ μm, $100 < \varepsilon < 250$ μm and $\varepsilon < 100$ μm, each of one characterising a different corrosion rate of the Fe-36Ni alloy:

- for $\varepsilon > 250$ μm, the experimental points fall on within a straight line, indicating a corrosion rate proportional to the electrolyte thickness (ε).

- for $100 < \varepsilon < 250$ μm, a faster increase of R_t is observed, revealing a decrease of the corrosion rate. It should be of interest to take again the calculated value of the layer thickness corresponding to the saturation in $FeSO_4$; the thickness thus found was 150 μm. The examination of the $R_t = f(\varepsilon)$ curve indicates that this thickness coincides with the beginning of the R_t increase; this time corresponds to that moment when a protective layer develops at the surface. In this thickness range, the system is presumably governed by a mixed kinetics phenomenon (diffusion-confinement).

- for $\varepsilon < 100$ μm, the diffusion process of the corrosion products towards the outside of the thin layer becomes negligible. In other words, the products of the electrochemical reaction are confined in the thin layer which is characterised by a decrease of R_t. This result confirms the mechanism quantitatively evoked while studying the anodic polarisation curve.

III. Conclusion

The variation of the electrochemical impedance as a function of the frequency range related to the current-potential characteristic could allow to identify the corrosion process of the Fe-36Ni alloy covered by a thin electrolyte layer. For instance the results depicted in this paper have obviously shown three critical regions:

- A bulk solution section where the corrosion rate appears to be relatively constant while $\varepsilon > 500$ μm.

- A decrease of the corrosion rate seemingly caused by a partial control transport process while $100 < \varepsilon < 500$ μm.

- And finally when $\varepsilon < 100$ μm, a region in which the confinement of the corrosion products becomes major with regard to their diffusion towards the outside of the thin layer. This therefore leads to an acceleration of the corrosion rate which enlightens the abrupt diminution of R_t at the small electrolyte thickness values. This result is indicated by the absence of activation peak observed while considering the anodic polarisation curve of the Fe-36Ni alloy.

REFERENCES

1. I. L. Rozenfeld, Atmospheric corrosion of metals, Nace Publications, Houston (1972)

2. P. P. Phipps and P.W. Rice, in the chemistry of corrosion. A.C.S. Publication (1972)

3. H. W. Pickering, Corr. Sci ., 29, 325 (1989)

4. E. Mc. Cafferty, J. of Electrochem. Soc. 126, 3, 385 (1979)

5. G. A. El-Mahdy, Atsushi Nishikata, Tooru Tsuru, Corr. Sci., 42, 1509-1521 (2000)

6. Y. Xu and H. W. Pickering, J. Electrochem. Soc. 140, 3, 658 (1993)

7. E. A. Nystrom, J. B. Lee, A. C. Sagüés, H. W. Pickering, J. of Electrochem. Soc.141, 2, 359 (1994)

8. M. Watson and J. Postlethwaite , Corr. 46, 7, 522 (1990)

9. A. J. Betts, L. H. Boulton , British. Corr. J. 28, 4, 279 (1993)

10. R. D. Klassen, P. R. Roberge, C. V. Hyatt, Electrochimica Acta 46, 3705-3713 (2001)

11. C. Fiaud, A. Kadri, Materiels Chemistry and physics, 9, 529 (1983)

12. R. Abbeg, Handbuch der Anorganishen Chemie Verlag Iron,S. Hirzel Leipzig, B56, (1930)

13. R. De Levie, Advance in electrochemistry and electrochemical engineering, Ed. P. Delahay, Vol. VI , 329 , Interscience New York (1967).

14. H. Keiser , K.D. Beccu, M.A. Gutjahr, Electrochem. Acta , 21, 539 (1976)

15. J.P. Candy, P. Candy, P. Fouilleux, Electrochemica Acta 26, 8, 1029 (1981)

16. M. Keddam, C. Rakotomavo, H. Takenouti, J. of Applied Electrochemistry 14, 437 (1984)

17. C. Fiaud, R. Chahrouri, M. Keddam, G. Maurin, H. Takenouti, 8th International Congress on Metallic Corrosion, Mayence (RFA) sept. (1981)

18. C. Fiaud, M. Keddam, A. Kadri, H. Takenouti Electrochemica Acta 32, 3, 445 (1987)

19. C. Gabrielli and M. Keddam Corr. 48, 10, 794 (1992)

Figures Caption

Figure 1. Cell arrangement showing the thin electrolyte layer device. Electrolytic connection to the reference electrode with capillary tip outside the thin layer.

Figure 2. Anodic polarisation curves of Fe 36Ni alloy under thin layer of (Na_2SO_4+ H_2SO_4) pH = 2.9

Figure 3. Impedance diagrams in the complex plane of an Fe-36Ni electrode at various layer thikness.

Figure 4. Impedance diagram selected from Figure 3, layer thickness (ε = 20 μm) , showing the definition of Re, RD and Rt.

Figure 5. Linear relationship between the reciprocal of the electrolyte resistance Re and the electrolyte layer thickness

Figure 6. Magnification of the high frequency range of the impedance diagrams of Fe-36Ni electrode at various layer thickness of electrolyte (pH= 2.9)

Figure 7. I = f (V) characteristics as a function of the electrolyte film thickness

Figure 8. Variation of $\Delta E/\Delta I = P$ as a function of the electrolyte layer. P is taken from figure 7.

Figure 9. Variation of transfert resistance Rt Vs the electrolyte film thickness.

ε_c : calculated value corresponding to the saturation of the layer by the corrosion product.

Tables Caption

Table 1. Characteristics of the anodic current-potential curves of the Fe-36Ni alloy under thin layer film of H_2SO_4 (pH=2.9). Effect of thickness ε on I_m and E_p.

Table 2. Concentration of the dissolved iron as a function of the layer electrolyte thickness

Table 3. Evolution of the corrosion potential $E_{corr.}$, R_e, R_D and P as a function of thickness ε. R_e : measured electrolyte equivalente resistance at 10 kHz, R_D : value deducted from the impedance measurements (fig. 3), P: $\Delta E/\Delta I$ slopes of the curves reported on figure 7 and ε electrolyte film thickness.

Table 4. Evolution of the electrolyte equivalente resistance R_e and transfer resistance R_t as a function of the electrolyte thickness ε.

Table 5. Evolution of the corrosion products concentration into the thin electrolyte layer deducted from the impedance measurements, according to the same principle of calculation than thus utilised for the table 3.

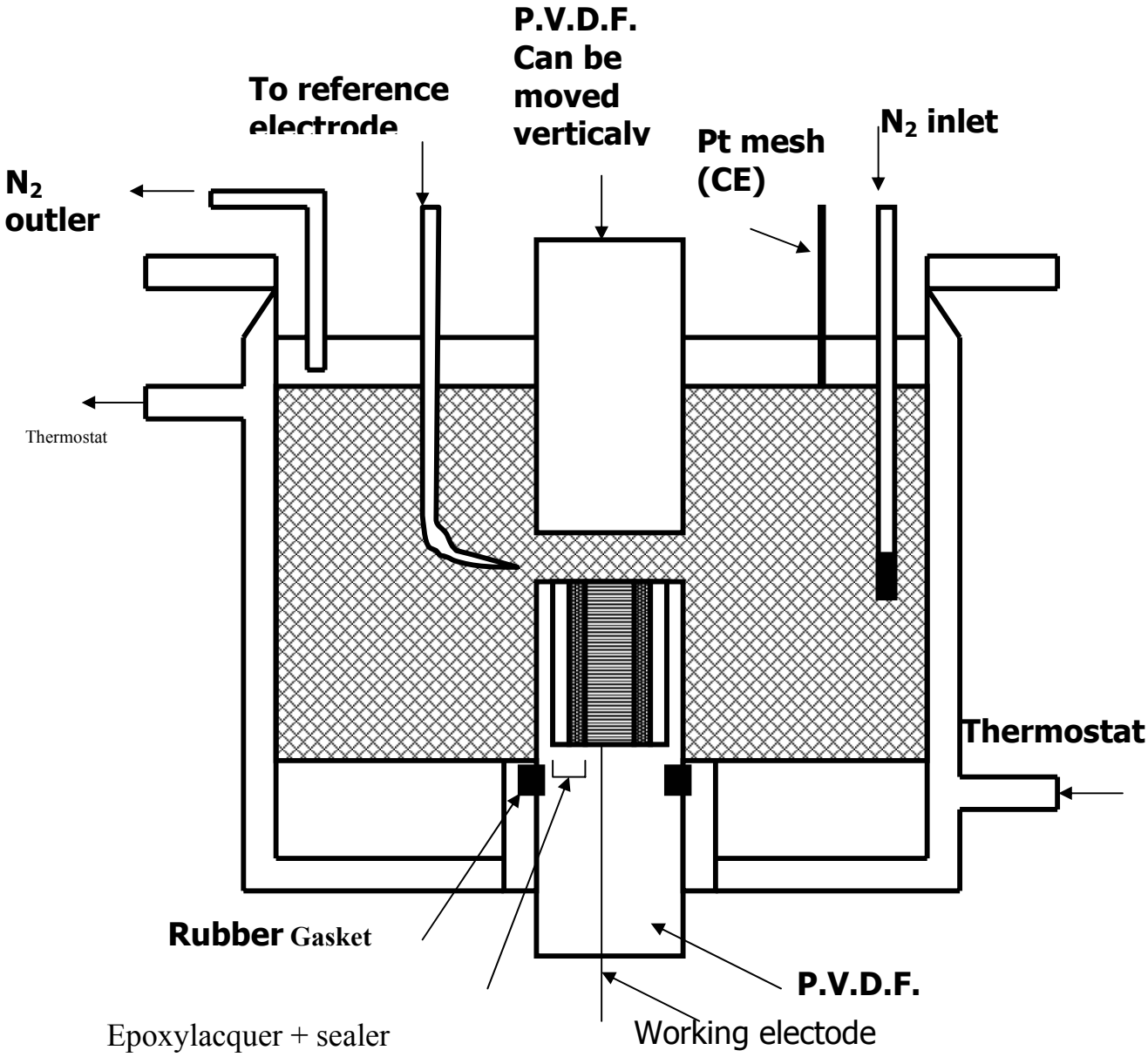
P.V.D.F.
Can be
moved
verticalv
To reference
electrode
Pt mesh
(CE)
N_2 inlet
N_2
outler
Thermostat
Thermostat
Rubber Gasket
P.V.D.F.
Epoxylacquer + sealer
Working electode

Figure 1

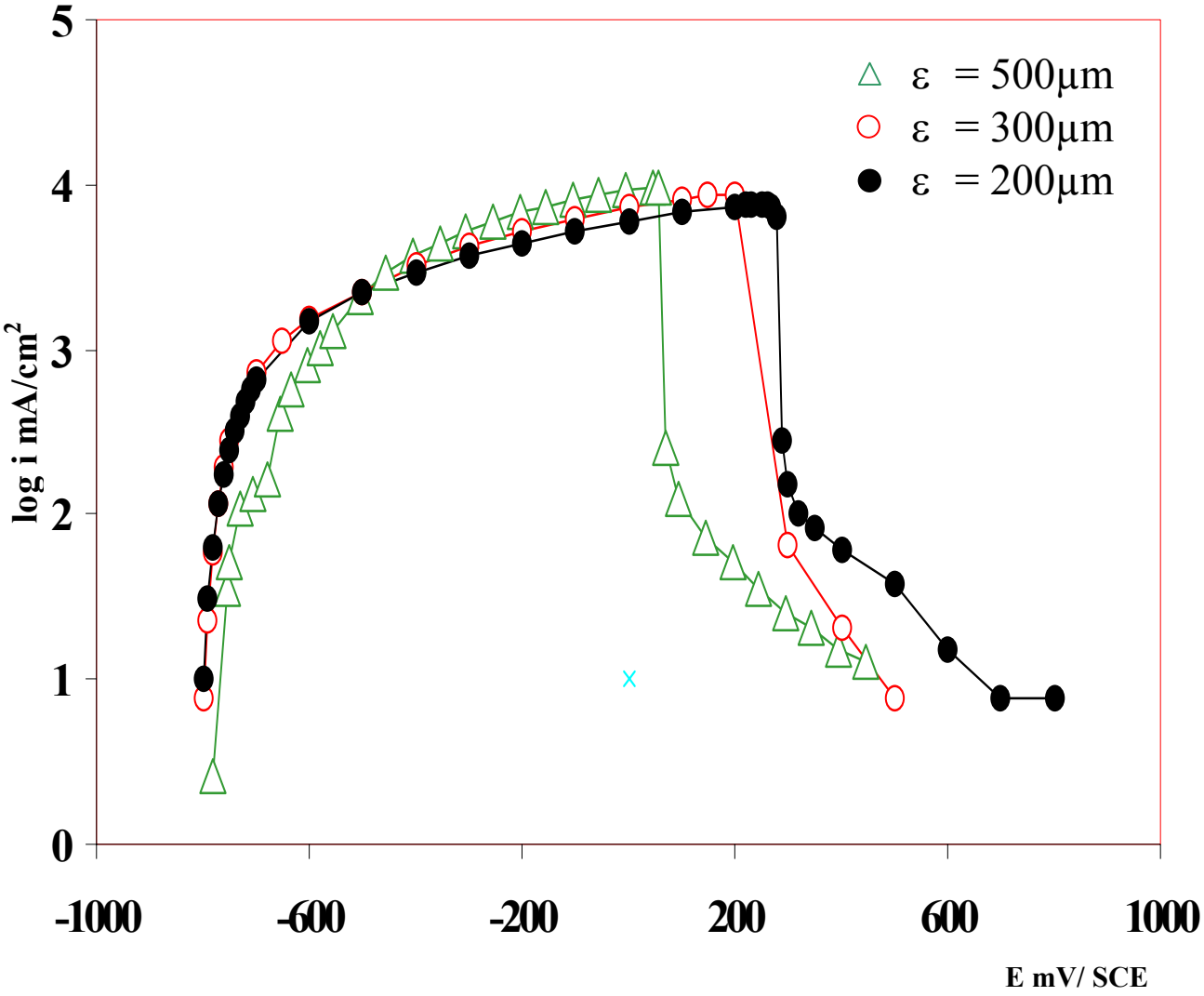
5
4
3
2
1
0
log i mA/cm2
-1000
-600
-200
200
600
1000
E mV/ SCE
ε = 500µm
ε = 300µm
ε = 200µm

Figure 2

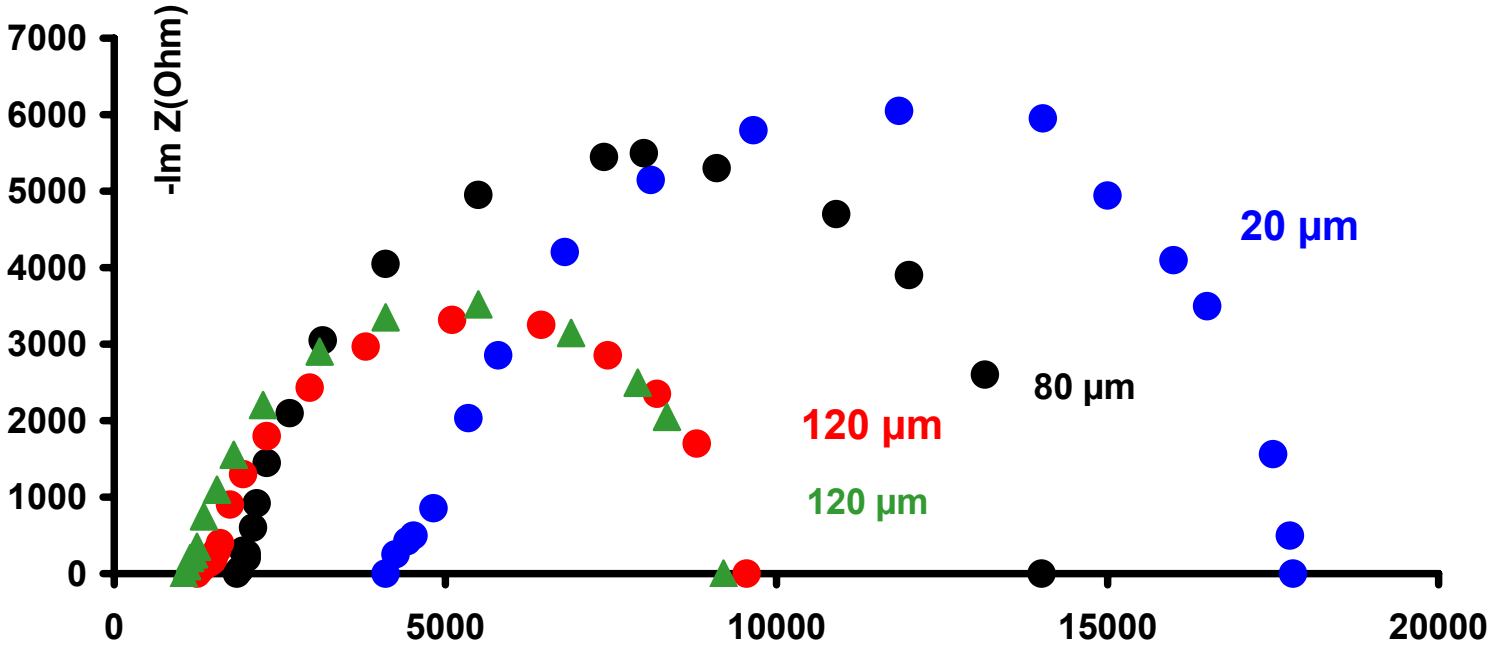
-Im Z(Ohm)
7000
6000
5000
4000
3000
2000
1000
0
0
5000
10000
15000
20000
20 µm
80 µm
120 µm
120 µm

Figure 3

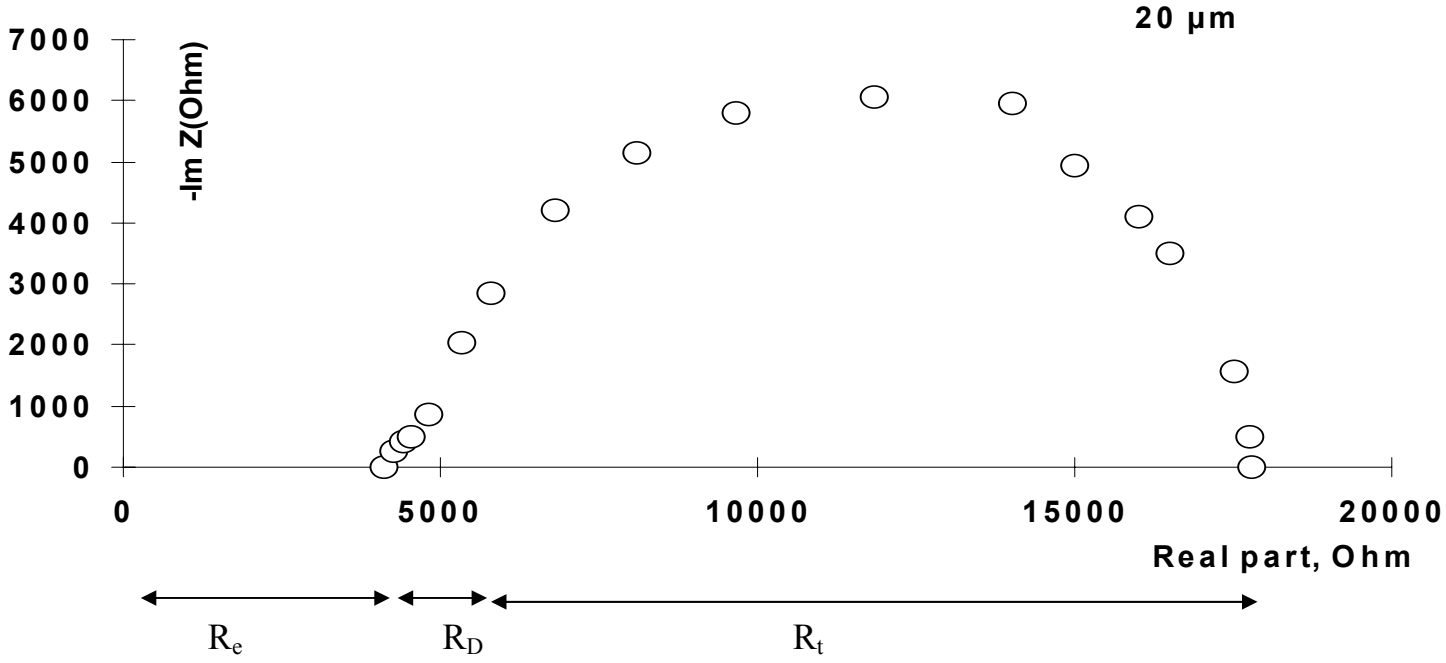
20 µm
7000
6000
5000
4000
3000
2000
1000
0
-Im Z(Ohm)
0
5000
10000
15000
20000
Real part, Ohm
R_e
R_D
R_t

Figure 4

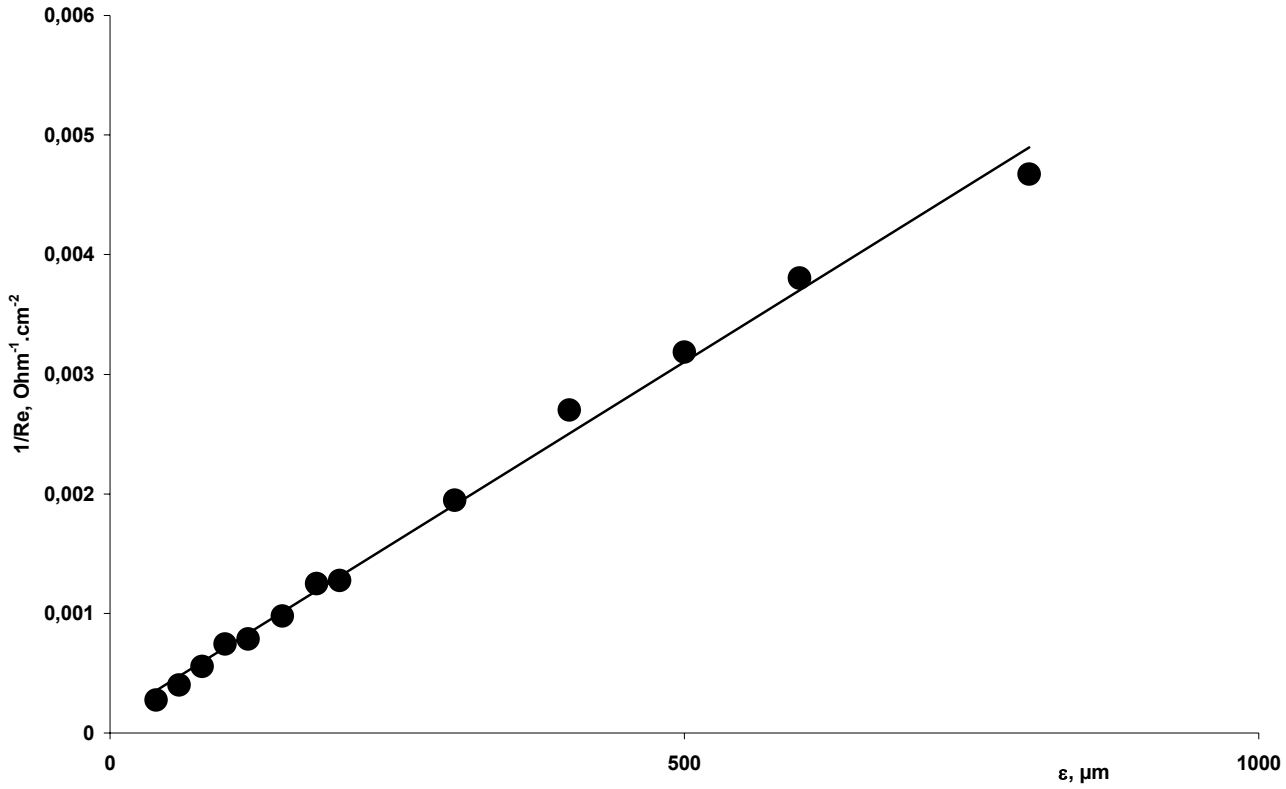

Figure 5

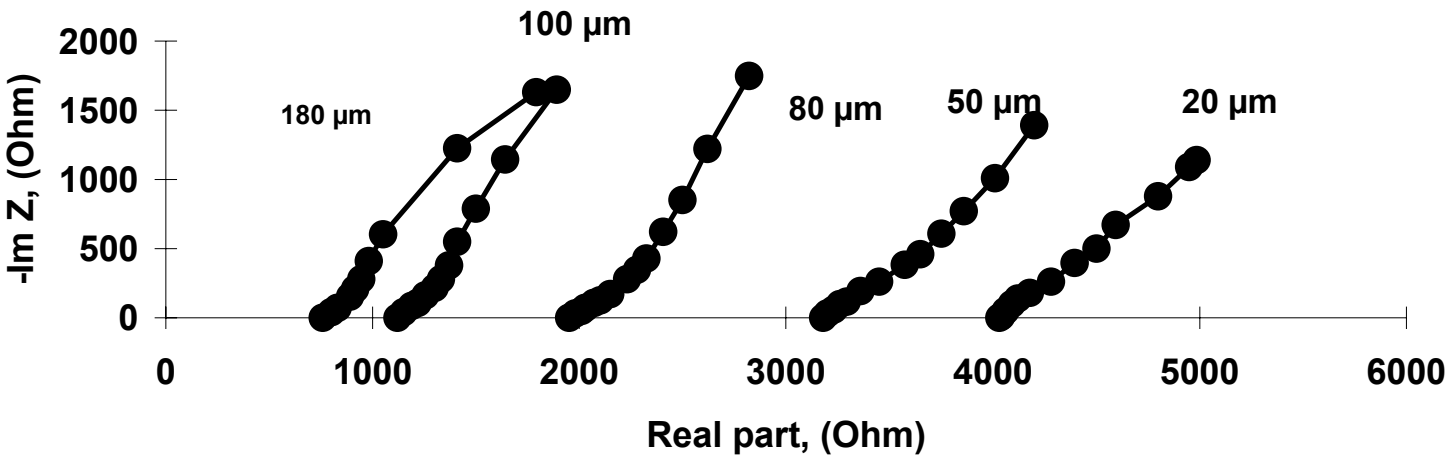
100 µm
180 µm
80 µm
50 µm
20 µm
-Im Z, (Ohm)
2000
1500
1000
500
0
0
1000
2000
3000
4000
5000
6000
Real part, (Ohm)

Figure 6

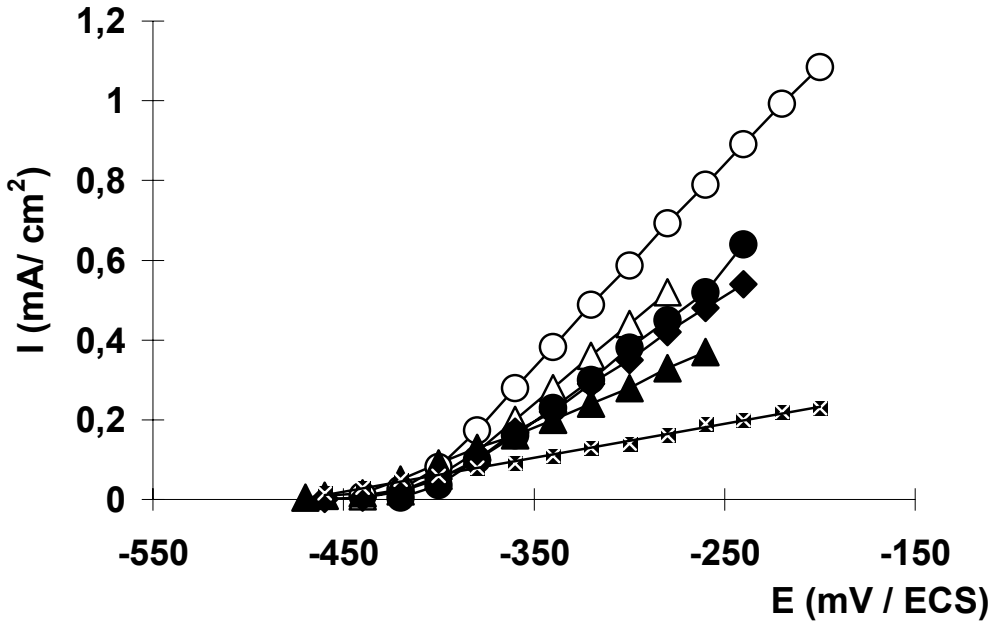

Figure 7

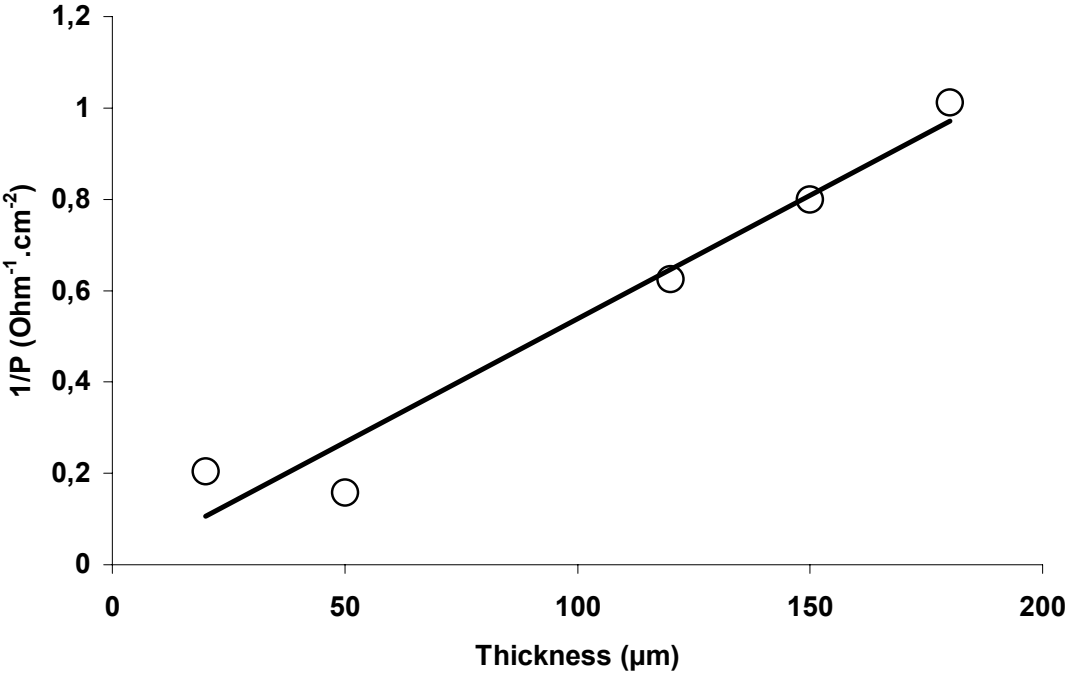

Figure 8

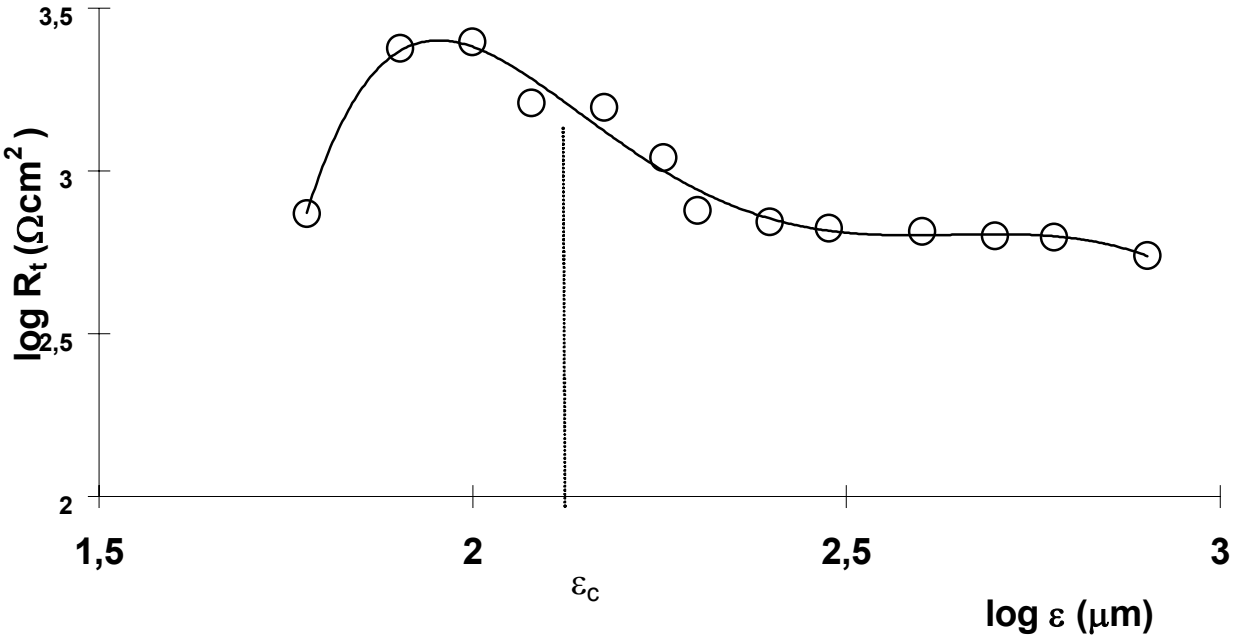

Figure 9

Layer thickness of electrolyte (μm)	Electrolyte volume in the thin layer (μl)	scanning speed mv/sec	Current density of the actavation peak I_m mA/cm^2	Potential Activation peak mV/SCE
1000	314	0.5 2 5	14.5 19.4 21.1	266 275 235
500	157	0.5 1 2 5	11 9.73 16 17.2	490 570 555 605
300	94	0.5 1	8.8 8.7	450 600
200	62.8	0.5 1 10	10.8 7.58 9.8	1080 650 855
150	47	5 10	9.6 9.8	955 1155
100	31.4	5	9.6	1030

Table 1

Layer thickness of electrolyte ε (μm)	Electrolyte volume (μl)	ϕ_R (mole/ sec)	C mole/ litre
500 **300** **200** **100**	157 94 62.8 31.4	$4.3\ 10^{-10}$ $8.6\ 10^{-10}$ $7.7\ 10^{-10}$ $1.8\ 10^{-9}$	$14\ 10^{-2}$ $46\ 10^{-2}$ $59\ 10^{-2}$ $29\ 10^{-1}$

Table 2

ε (μm)	$E_{corr.}$ (mV/ ECS)	R_e (kΩ)	R_D (kΩ)	$R_e + R_D$ (kΩ)	P (kΩ)
180	-455	0.80	0.290	1.09	0.988
150	-461	1.020	0.360	1.38	1.25
120	-466	1.270	0.440	1.71	1.60
50	-480	2.80	0.900	3.70	6.32
40	-490	3.64	0.735	4.37	4.88
20		4.13	1.03	5.16	

Table 3

ε (μm)	R_e (kΩ)	R_t ($\Omega . Cm^2$)
800	0.214	550
600	0.263	626
500	0.314	634
400	0.370	652
300	0.514	668
200	0.785	756
180	0.800	1100
150	1.020	1570
120	1.270	1620
100	1.340	2500
80	1.800	2390
60	2.500	740
40	3.640	870

Table 4

ε (μm)	R_t I_{corr} (V)	$I_{corr.}$ (A)	$\varnothing_R$ (mole / sec)	C (mole / l)
500	0.03	$9{,}46 \cdot 10^{-6}$	$4{,}9 \cdot 10^{-11}$	$1{,}6 \cdot 10^{-2}$
400	0.03	$9{,}2 \cdot 10^{-6}$	$4{,}8 \cdot 10^{-11}$	$2{,}0 \cdot 10^{-2}$
300	0.03	$8{,}98 \cdot 10^{-6}$	$4{,}65 \cdot 10^{-11}$	$2{,}5 \cdot 10^{-2}$
200	0.03	$7{,}94 \cdot 10^{-6}$	$4{,}11 \cdot 10^{-11}$	$3{,}3 \cdot 10^{-2}$
100	0.03	$2{,}4 \cdot 10^{-6}$	$1{,}24 \cdot 10^{-11}$	$2{,}0 \cdot 10^{-2}$
60	0.03	$8{,}11 \cdot 10^{-6}$	$4{,}2 \cdot 10^{-11}$	$1{,}11 \cdot 10^{-1}$
40	0.03	$6{,}89 \cdot 10^{-6}$	$3{,}6 \cdot 10^{-11}$	$1{,}43 \cdot 10^{-1}$

Table 5